Shadow wave-function variational calculations of crystalline and liquid phases of ^{4}He

S. A. Vitiello and K. J. Runge
Courant Institute of Mathematical Sciences, New York University, New York, New York 10012

G. V. Chester
Laboratory of Atomic and Solid State Physics, Cornell University, Ithaca, New York 14853

M. H. Kalos
Courant Institute of Mathematical Sciences, New York University, New York, New York 10012

(Received 20 April 1989; revised manuscript received 9 November 1989)

A new class of variational wave functions for boson systems, shadow wave functions, is used to investigate the properties of solid and liquid ^{4}He. The wave function is translationally invariant and symmetric under particle interchange. In principle, the calculations for the crystalline phase do not require the use of any auxiliary lattice. Using the Metropolis Monte Carlo algorithm, we show that the additional variational degrees of freedom in the wave function lower the energy significantly. This wave function also allows the crystalization of an equilibrated liquid phase when a crystalline seed is used. The pair correlation function and structure factor $S(k)$ are determined in the liquid phase. The condensate fraction is calculated as well. Results are given for the single-particle distribution function around the lattice positions in the solid phase.

I. INTRODUCTION

In a previous paper[1] we proposed a new class of variational wave functions for many-body Bose systems. The aim was to compute the properties of solid and liquid ^{4}He at zero temperature. This new wave function takes into account some important characteristics that have been neglected in previous variational Monte Carlo calculations. It is symmetric under particle exchange and translationally invariant, even in the solid phase (for systems satisfying periodic boundary conditions, the true ground state has translational invariance). Also in the solid phase our wave function does not require the *a priori* introduction of a crystal lattice. It is therefore able to crystallize an initially equilibrated liquid system if an appropriate crystalline seed is introduced during the simulation. The new wave function contains to all orders enhanced correlations among particles when compared with the standard Jastrow form.[2] Recently, it has been proved by Reatto and Masserini[3] that our wave function has a Bose-Einstein condensate in both the liquid and solid phases.

In the new wave function, the particle coordinates are coupled to each other by a product of factors of the Jastrow form and to an auxiliary set of variables. These new variables interact among themselves by a model potential as if they were classical particles in the corresponding thermodynamic phase, either solid or fluid. Integrating out these auxiliary variables yields a wave function that depends only on the coordinates of the real particles. One may think of each auxiliary variable as the coordinate of a fictitious or "shadow" particle. We refer therefore to this class of wave functions as shadow wave functions. In this work we investigate in a systematic way the characteristics and consequences of the new class of wave functions as they pertain to the crystalline and liquid phases of ^{4}He. We stress that our main concern is in the improvements due to the introduction of shadow degrees of freedom. Therefore, the form of the pseudopotential for the real particles is chosen to be the simple one used by McMillan,[4] with no attempt to optimize it (see the following section). Although the pseudopotential functional form has not been optimized, we compare our results with other variational calculations in which more elaborate pseudopotentials or explicit three-body correlations have been used and also with some Green's-function Monte Carlo results.

In Sec. II we define the shadow wave function and give physical motivations for its introduction. Section III discusses the system under consideration, the form of the shadow wave function applied, and our method of analysis. Sections IV and V contain our results for the liquid and solid phases of ^{4}He, respectively. Our results for the crystallization of an equilibrated liquid phase obtained using a crystalline seed are presented in Sec. VI. In Sec. VII we present a summary and discussion of this work.

II. THE SHADOW WAVE FUNCTION

The variational shadow wave function $\Psi_T(R)$ for a system with N particles, $R \equiv \{\mathbf{r}_1, \mathbf{r}_2, \ldots, \mathbf{r}_N\}$ is constructed by considering a set of auxiliary or shadow variables $S \equiv \{\mathbf{s}_1, \mathbf{s}_2, \ldots, \mathbf{s}_N\}$ through

$$\Psi_T(R) = \int \Xi(R,S)dS \ . \tag{1}$$

The function $\Xi(R,S)$ used here is the product of three terms

$$\Xi(R,S) = \psi_R(R) \prod_k \theta(\mathbf{r}_k - \mathbf{s}_k)\psi_s(S) \ . \tag{2}$$

The factors ψ are of the Jastrow form; thus, for the real particles it is given by

$$\psi_r(R)=\prod_{i<j} e^{-(1/2)u(r_{ij})} , \tag{3}$$

where $r_{ij}=|\mathbf{r}_i-\mathbf{r}_j|$ is the distance between particles i and j. As mentioned above, the pseudopotential $u(r_{ij})$ used here has the McMillan form,[4]

$$u(r)=\left[\frac{b}{r}\right]^5 , \tag{4}$$

with b taken as a variational parameter. The second factor in Eq. (2), involving $\theta(\mathbf{r}_k-\mathbf{s}_k)$, provides a coupling between the particles and the shadows variables. In this work θ is chosen to be a Gaussian:

$$\theta(\mathbf{r}_k-\mathbf{s}_k)=e^{-C(\mathbf{r}_k-\mathbf{s}_k)^2} , \tag{5}$$

where C is a variational parameter. Finally, $\psi_s(S)$ is a Jastrow product that couples the shadow variables to each other and is written as

$$\psi_s(S)=\prod_{i<j} e^{-v(s_{ij})} , \tag{6}$$

where $s_{ij}=|\mathbf{s}_i-\mathbf{s}_j|$. The model potential $v(s_{ij})$ selected for the shadows is

$$v(s)=\left[\frac{b_{\rm sh}}{s}\right]^n , \tag{7}$$

and has two variational parameters $b_{\rm sh}$ and n.

A useful way of writing our trial wave function Eq. (1) is through the expression

$$\Psi_T(R)=\psi_r(R)\varphi(R) . \tag{8}$$

This equation is obtained through the substitution of Eq. (2) into Eq. (1) and then by integrating out the shadow variables, so that

$$\varphi(R)=\int \prod_k \theta(\mathbf{r}_k-\mathbf{s}_k)\psi_s(S)dS . \tag{9}$$

Inspection of $\varphi(R)$ shows that our trial wave function goes beyond the pairwise Jastrow form (3).

For boson systems in previous Monte Carlo calculations without explicit three-body correlations,[5] the model function $\varphi(R)$ was taken to be equal to 1 for the ground state of the liquid phase.[4] In the crystal phase it was taken as a product of Gaussians[6,7] centered about an *a priori* chosen lattice. This last procedure, although it yielded reasonable trial energies, destroyed some of the known properties of the wave function, viz., translational invariance and symmetry under particle exchange. The wave function used in the present work restores these properties.

The role of the model function $\varphi(R)$ can be elucidated by the following arguments. The first involves interpreting the sum over all paths in imaginary time for quantum systems.[8] Here it is useful to reinterpet the system's (low-temperature) partition function in Feynman's formulation as a classical system of N interacting polymers.[9,10] The action is a sum of the average potential and kinetic energies along the path, the latter being represented by an intrapolymer harmonic interaction between adjacent monomers. The path of any particle may be decomposed into the center of mass (or average position) and fluctuations about this point. The fluctuation may be thought of as due to quantum uncertainty. Some of the properties of these centers of mass have been studied[11] in quantum Yukawa systems. In path-integral Monte Carlo investigations[12] of the hard-sphere system we have found that monitoring the structural properties of the centers of mass aids in the interpretation of the simulation results. In the shadow wave function, one can think of each shadow coordinate $\mathbf{s}_k$ as the "center of mass" of the path corresponding to particle k. Furthermore, the average in the path integral over fluctuations about the center of mass results in a "dressed" interaction between the centers. This interaction should be reflected in a rather large repulsion at short distances between centers of mass and therefore its correlation should have more structure than the real particles. Thus the centers of mass behave more like classical particles. Our results support this view. The particle-shadow interaction, $\theta(\mathbf{r}_i-\mathbf{s}_i)$, in our wave function may be thought of as a model for the fluctuations of the coordinate along the path with respect to their center of mass. As a first approximation it may be taken as a Gaussian since the intrapolymer interaction in the path integral is harmonic.

Secondly, because a squared product of the Jastrow form can be formally identified with the Boltzmann factor of some classical system, the Jastrow product should correspond to a solid when the correlation between the particles in the wave function is increased sufficiently. However, if a trial wave function of this form is used for a quantum crystal, it is well known[6] that, although a solid is formed, the energy is much too high and the pair correlation function is unacceptable. These poor results are due to the conflict between the necessity of solving the quantum two-body problem for small pair separations r, and the requirement of low "effective temperatures" for crystallization. A phenomenological way to reconcile these two different aspects of the problem is by the use of the shadow wave function. The part of the wave function, ψ_s, associated with the shadow particles provides the interaction necessary for solidification, while the part, ψ_r, associated with real particles, allows for the correct behavior at small r.

The final motivation for the shadow wave function is found by considering the Green's-function Monte Carlo (GFMC) method.[13,14] In this method, the integral form of the Schrödinger equation,

$$\Psi(R)=E\int G(R,S)\Psi(S)dS , \tag{10}$$

is solved for the ground state by iteration, where $G(R,S)$ is the operator corresponding to the inverse of the system Hamiltonian H. In this context the shadow wave function can be thought of as a first iteration of a system described by a single Jastrow product of two-body correlation $f_0(\mathbf{s}_i-\mathbf{s}_j)$. To see how this interpretation can be made let us assume the following approximation for the

Green's function. $G(R,S)$ is taken as the free-particle Boltzmann Green's function of an effective temperature "dressed" by Jastrow factors, $f_1(R)$ and $f_1(S)$, to model the correlations of the interacting system:

$$G(R,S) \propto \prod_{i<j} f_1(\mathbf{r}_i-\mathbf{r}_j) \prod_k e^{-C(\mathbf{r}_k-\mathbf{s}_k)^2} \times \prod_{l<m} f_1(\mathbf{s}_l-\mathbf{s}_m) . \quad (11)$$

This expression for $G(R,S)$ has the correct symmetry properties in R and S. Also it should approximately satisfy the Green's-function relation $\int H(R)G(R,S)dS \approx$ const. From the substitution of this approximate form for $G(R,S)$ into Eq. (10) one can see that a wave function of the shadow form results.

III. METHOD OF ANALYSIS

The Hamiltonian of N ^{4}He atoms with mass m is taken as

$$H=-\frac{\hbar^2}{2m}\sum_{i=1}^{N}\nabla_i^2+\sum_{i<j}V(r_{ij}) . \quad (12)$$

The two-body potential $V(r_{ij})$ used here is the accurate one proposed by Aziz *et al.*[15] This potential has been extensively used and has yielded excellent results.[16]

The true ground-state energy has an upper bound given by

$$E_0 \le E_T=\frac{\int dR\,\psi_T\Psi_T}{\int dR\,|\Psi_T|^2} . \quad (13)$$

This equation can be rewritten in terms of Eqs. (1) and (2) so that it reads

$$E_T=\int\int\int dR\,dS\,dS' p(R,S,S') \left[H\psi(R)\prod_k \theta(\mathbf{r}_k-\mathbf{s}_k') \Big/ \psi(R)\prod_k \theta(\mathbf{r}_k-\mathbf{s}_k') \right] , \quad (14)$$

where $p(R,S,S')$ is given by

$$p(R,S,S')=\frac{\Xi(R,S)\Xi(R,S')}{\int\int\int dR\,dS\,dS'\Xi(R,S)\Xi(R,S')} . \quad (15)$$

The $9N$ dimensional integral in Eq. (14) is evaluated by the Metropolis Monte Carlo algorithm.[17] In this method the probability density function $p(R,S,S')$ is sampled and the estimator

$$\left[H\psi(R)\prod_k \theta(\mathbf{r}_k-\mathbf{s}_k') \Big/ \psi(R)\prod_k \theta(\mathbf{r}_k-\mathbf{r}_k') \right]$$

is averaged using the configurations generated in the random walk. To sample $p(R,S,S')$, the Metropolis steps are subdivided in two parts. In the first, one attempts to move real coordinates at random inside cubical boxes of side length Δ. In the second, analogous attempts to move shadow coordinates are made inside cubical boxes of side length Δ_{sh}. The moves are accepted with the probability

$$q=\min\left[1,\frac{p_{new}}{p(R,S,S')}\right] , \quad (16)$$

where p_{new} is the new value of the probability density function in Eq. (15) with one of its coordinates displaced. Details of the modifications of the Metropolis Monte Carlo algorithm necessary to deal with the shadow wave function can be found elsewhere.[18] The parameters Δ and Δ_{sh} are adjusted so that the acceptance is about 50%.

In addition to the ground-state variational energy, the radial distribution function $g(r)$, its Fourier transform, the structure factor $S(k)$, and single-particle distribution function $\rho(r)$ for displacements from a lattice site have been computed. These quantities are spherical averages and have been computed for both the real particles and the shadow coordinates. The condensate fraction n_0 has been computed as well.

The two-body distribution function is defined by

$$g(r)=\frac{1}{N\rho}\sum_{i\neq j}\langle\delta(|\mathbf{r}_i-\mathbf{r}_j-\mathbf{r}|)\rangle . \quad (17)$$

The angular brackets denote an average with respect to $|\Psi_T|^2$. The Fourier transform of $g(r)$ is the structure factor $S(k)$ and is given by

$$S(k)=1+\frac{\rho}{2}\int e^{i\mathbf{k}\cdot\mathbf{r}}[g(r)-1]d\mathbf{r} . \quad (18)$$

This quantity is also related to fluctuations with wave vector k about the average particle density $\rho_k=\sum_j e^{-i\mathbf{k}\cdot\mathbf{r}_j}$ by

$$S(k)=\frac{1}{N}\langle\rho_k^\dagger\rho_k\rangle . \quad (19)$$

The computation of the condensate fraction n_0, a measure of the off-diagonal long-range order (ODLRO), is of special interest. Following Penrose and Onsager,[19] it measures the extent to which a type of Bose-Einstein condensation happens below T_λ, the temperature for the lambda transition. It characterizes the macroscopic occupation of the zero-momentum state of the superfluid phase of a Bose system. The single-particle density matrix $n(r)$ at $r=|\mathbf{r}_i'-\mathbf{r}_i|$ is defined as

$$n(r)=\frac{\int dR\,\Psi_T(\mathbf{r}_1,\mathbf{r}_2,\ldots,\mathbf{r}_i',\ldots,\mathbf{r}_N)\Psi_T(\mathbf{r}_1,\mathbf{r}_2,\ldots,\mathbf{r}_i,\ldots,\mathbf{r}_N)}{\int dR|\Psi_T(R)|^2} . \quad (20)$$

Clearly $n(0)=1$. The fraction of particles in the zero-momentum state is given by

$$n_0=\lim_{r\to\infty} n(r) . \tag{21}$$

The standard way[4] of computing $n(r)$ is to consider equilibrated configurations of the diagonal density matrix and then take the average

$$n(r)=\left\langle \frac{\Psi_T(\mathbf{r}_1,\mathbf{r}_2,\ldots,\mathbf{r}_i+\mathbf{r},\ldots,\mathbf{r}_N)}{\Psi_T(\mathbf{r}_1,\mathbf{r}_2,\ldots,\mathbf{r}_i,\ldots,\mathbf{r}_N)} \right\rangle , \tag{22}$$

where $\mathbf{r}_i+\mathbf{r}$ could be any point inside the system.

In the solid phase an important quantity is the single-particle distribution function for displacements from a lattice site,

$$\rho(r)=\langle \delta(|\mathbf{r}_i-\mathbf{l}_i-\mathbf{r}|)\rangle , \tag{23}$$

where $\mathbf{l}_i$ is the coordinate of the ith lattice site corrected for the drift in the center of mass that occurs during the course of the simulation. Recall that these calculations do not rely on a lattice introduced *a priori*. We discuss the results for the liquid and solid phases in the following sections.

IV. THE FLUID PHASE

We have investigated the properties discussed above of ^{4}He in the fluid phase at the equilibrium density $\rho\sigma^3=0.365$ and at $\rho\sigma^3=0.437$ ($\sigma=2.556$ Å). The latter is the freezing density computed by the GFMC method.[16] Our calculations started from a fcc lattice, for both the real and the shadow particles. The equilibrium state of the system as liquid was quickly obtained for the particles and shadows at both densities. This behavior is readily seen by observing the evolution of $S(k)$. Although we have allowed much longer equilibrations, as few as 100 "passes" for the small system were enough to obtain a typical liquid value of $S(k)$ (cf. Fig. 7). The variational energies per atom for a system of 108 particles at the two densities are shown in Table I. At the lower density the power law of the shadow coordinates' Jastrow factor has been varied; cf. Eq. (7). One sees that there is a slight improvement in the energy when $n=9$ in that equation. In the second column of Table II we display the variational energy per atom computed at $\rho\sigma^3=0.365$ for the pure Jastrow wave function. The only variational parameter in this calculation is b; cf. Eq. (4). Its optimum value is given by $b=1.20\sigma$. As we can see the shadow wave function provides a 0.4 K reduction in the variational energy when compared with a function of a pure Jastrow form. Also in Table II, we quote results from variational calculations obtained with other trial functions, and results using the GFMC method.

TABLE I. Variational energies in K per atom obtained with the shadow wave function for the liquid phase at the equilibrium and freezing densities. The b and C parameters are given in units of σ and σ^{-2}, respectively ($\sigma=2.556$ Å).

		Parameters			
$\rho\sigma^3$	E_T	b	b_{sh}	n	C
0.365	−6.061±0.025	1.13	1.40	5	4.0
0.365	−6.241±0.035	1.13	1.20	9	4.0
0.365	−6.133±0.048	1.13	1.16	12	4.0
0.438	−5.360±0.035	1.12	1.55	5	4.0

In the third column of Table II we quote results from the literature,[16] and in the last one we give unpublished results of P. Whitlock. The variational computations were performed using three different trial wave functions. The first of such calculations considered a functional optimization of the Jastrow factors by the paired-photon analysis (PPA) method as described by Pinski and Campbell.[20] This is followed by the variational energy per atom computed with a trial function of a pure Jastrow form together with explicit triple correlations as suggested by Schmidt *et al.*[5] The next line shows the same quantity obtained by the optimization of the Jastrow factor using PPA plus an explicit triplet term. In this case, the parameters of the triplet term have not been optimized; the parameters were the same as in the previous trial function. All the terms that did not include a functional optimization by PPA used the McMillan form, Eq. (4), for the Jastrow factors. In the two last lines we give a results obtained by the GFMC method. The one quoted

TABLE II. Results for liquid ^{4}He at the equilibration density, $\rho\sigma^3=0.365$, determined using a pure Jastrow (J) trial wave function, a functional optimization of the Jastrow factor by paired-phonon analysis [J(PPA)], Jastrow together with explicit three-body correlations ($J+T$), and a Jastrow in which the correlation factor is optimized by paired-phonon analysis and explicit triplet correlations [J(PPA)$+T$]. Besides these variational results we give, in the last two lines, the "mixed" energy estimator obtained by the Green's-function Monte Carlo (GFMC). The calculations have been performed for systems of 108 particles, except the ones using J(PPA) where 64 particles were considered. Units are the same as those of Table I.

Trial or importance function	This work	Energies Ref. 16	Ref. 28
		Variational	
J	−5.717±0.021		
J(PPA)		−5.87	−5.93±0.01
$J+T$			−6.674±0.007
J(PPA)$+T$			−6.741±0.008
		GFMC	
J(PPA)		−7.120±0.024	
$J+T$			−7.110±0.040

from the literature uses as importance function a functional optimization of the Jastrow wave function by the PPA method. Whitlock's unpublished result has been obtained using an important function that included explicit triple correlations for the first time. Note that this new GFMC result is in excellent agreement with the one previously published.

In this paper we will be quoting results obtained with the GFMC method using "mixed" and "extrapolated" expectations.[21] The meaning of these averages can be easily understood. In an importance sampled GFMC calculation with a trial function $\Psi_T(R)$, in the asymptotic regime one obtains configurations drawn from the distribution $\Psi_T\Psi_0$, where $\Psi_0(R)$ is the lowest energy eigenfunction that is not orthogonal to Ψ_T. For an operator F the mixed expectation is defined as

$$\langle F\rangle_M=\frac{\int\Psi_0(R)F\Psi_T(R)dR}{\int\Psi_0(R)\Psi_T(R)dR}\ . \tag{24}$$

It is possible to determine an approximate relation between

$$\frac{\int\Psi_0(R)F\Psi_0(R)dR}{\int\Psi_0(R)\Psi_0(R)dR} \tag{25}$$

and the mixed expectation value. To extract the exact result, we assume that the trial function Ψ_T differs from the ground-state wave function by a small amount $\epsilon\Psi$ so that we can write

$$\Psi_0=\Psi_T+\epsilon\Psi\ . \tag{26}$$

Substituting this expression (26) for Ψ_0 in (25), expanding on ϵ and neglecting terms of the order of $O(\epsilon^2)$ we get the extrapolated expectation

$$\langle F\rangle_X=2\langle F\rangle_M-\langle F\rangle_T\ , \tag{27}$$

where $\langle F\rangle_M$ is defined in Eq. (24) and $\langle F\rangle_T$ is the variational expectation computed with Ψ_T.

An insight of how well the shadow wave function describes the real system can be achieved by making a comparison between Tables I and II. If we compare our best energy at $\rho\sigma^3=0.356$ with the GFMC result we see that our trial function gives an energy 0.9 K higher. At the same time we see that the shadow wave function does better than the variational calculation with a functional optimization of the Jastrow factors by paired-phonon analysis. The results obtained with explicit three-body interactions show that our new trial function contains implicitly part of these important correlations. Our wave function is not quite as good in that it lowers the energy by only 0.5 K relative to the pure Jastrow while the wave function with explicit three-body correlations achieves a 1.0 K decrease.

The pair correlation functions $g(r)$ at the freezing density, $\rho\sigma^3=0.438$, for both real and shadow particles are plotted in Fig. 1. The maximum of $g(r)$ for the real particles, 1.396 ± 0.004, obtained at $r=1.38\sigma$ is 0.14 lower than the value determined using the GFMC method,[16] 1.5401, for $r=1.30\sigma$. The comparison between the pair

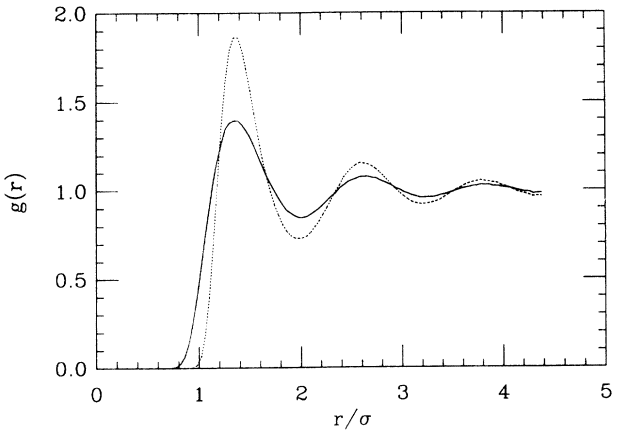

FIG. 1. Two-body correlation function for the liquid at the freezing density $\rho\sigma=0.438$ for the real particles, solid line. The dashed line shows the pair correlation function for the shadow coordinates at the same density.

correlation functions for the shadow particles obtained at three different densities (one in the crystalline phase) is made in Fig. 2. It is interesting to note that as we go to higher densities the structure of the shadow particles increases.

The structure function has been computed at the equilibrium density by two methods. In the first, one simply measures $S(k)$ directly as is given by Eq. (19), where k is a Born–von Karman wave vector consistent with the periodicity of the simulation cell. Here $S(k)$ is obtained on a discrete set of k's. In the second method, one fits the tail of $g(r)$ to a sum of (one to three) damped oscillations of the form $(A/r)e^{-ar}\cos(ar+b)$ as discussed by Ceperley and Chester.[22] With L the width of the simulation

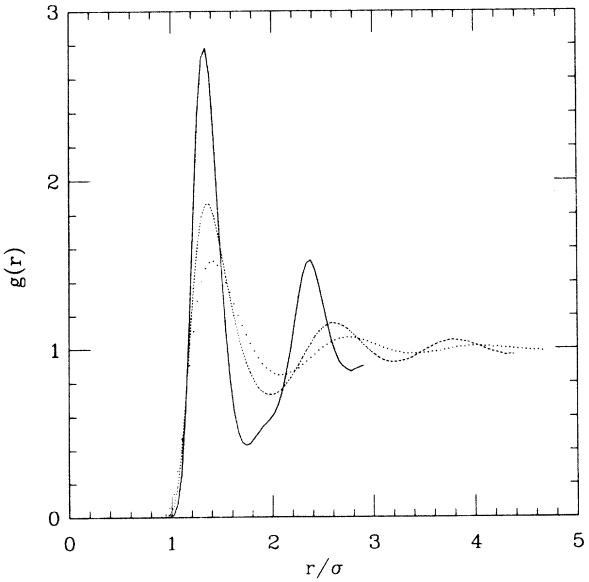

FIG. 2. Comparison between pair correlation functions for the shadow coordinates in the crystalline phase, $\rho\sigma^3=0.55$, solid line; the freezing density, $\rho\sigma^3=0.438$, dashed line; and at the equilibrium density, $\rho\sigma^3=0.365$, dotted line. At the highest density, $\rho\sigma^3=0.55$, the crystal structure in $g(r)$ is apparent.

cell, one then uses the Monte Carlo results for $g(r)$ when $r < L/2$ along with the damped oscillation fit when $r > L/2$ to perform a numerical Fourier transform of $g(r)$ as in Eq. (18). We show the results of both methods for the real particles in Fig. 3 and for the shadows in Fig. 4. In both cases the power law for the pseudopotential for the shadow coordinates is taken equal to 9, as in Eq. (7).

Our value for $S(k)$ at its maximum value in $k\sigma \approx 5.06$, as obtained from the Fourier transform of $g(r)$, is in excellent agreement with the GFMC result.[16] Variationally we obtained the value 1.356 for its maximum. The number obtained from GFMC calculations is 1.35. Both of these values are in agreement with the experimental data. In neutron diffraction experiments[23] at saturated vapor pressure at 1 K, which presumably gives results very near those at $T=0$, the maximum of $S(k)$ is 1.387 at $k\sigma \approx 5.24$. Determination of this maximum by x-ray[24] scattering at 1.16 K at a density close to saturated vapor pressure gives the value 1.3394 at $k\sigma \approx 5.28$.

As mentioned above, the structure of both the real and shadow coordinates increases with increasing density. We find at the freezing density ($\rho\sigma^3 = 0.438$) that the maximum in $S(k)$ is 1.55 for the real particles and 2.1 for the shadow particles. In classical systems it has been observed that freezing occurs when the maximum in $S(k)$ reaches 2.85 ± 0.1.[25] Although the structure in the shadow coordinates at freezing is not this high it is substantially closer than the corresponding value for the real coordinates. Further investigation is necessary to explore whether the correlations between the shadow particles contain a counterpart in quantum systems of the precursors associated with the freezing of classical liquids.

To compute the single-particle density matrix $n(r)$, we first used Eq. (22), As expected, this equation gives reliable values only for small values of r, up to 1σ. This results from the Gaussian interaction of the real particles with the shadow ones; cf. Eqs. (1), (2), and (5). In the calculation of $n(r)$, elements of the density matrix enter that are increasingly far from the diagonal, so that this Gaussian factor rapidly decreases the ratio in Eq. (22). A proper way of doing this calculation for any r should include a mechanism to allow the relaxation of the shadow particles. For small values of r, the coupled real and shadow particles will usually be near to each other, so that reasonable results will be obtained.

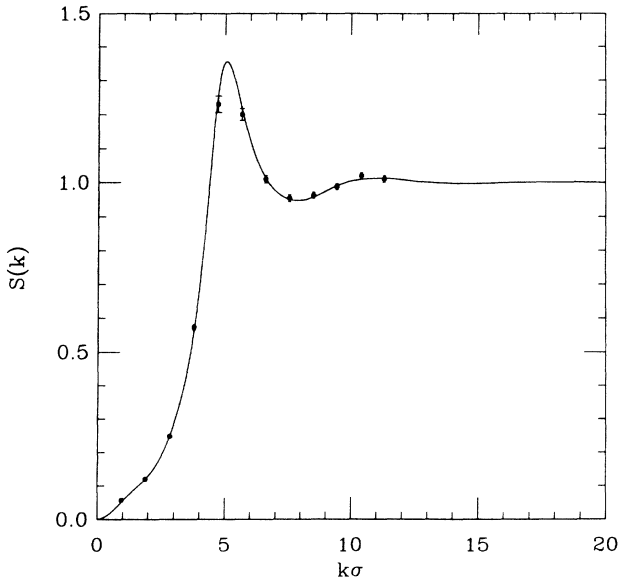

FIG. 3. Structure factor $S(k)$ for the real particles at $\rho\sigma^3 = 0.365$. The solid line is obtained by the Fourier transform of $g(r)$. The data with error bars is obtained directly from the configurations, cf. Eq. (19).

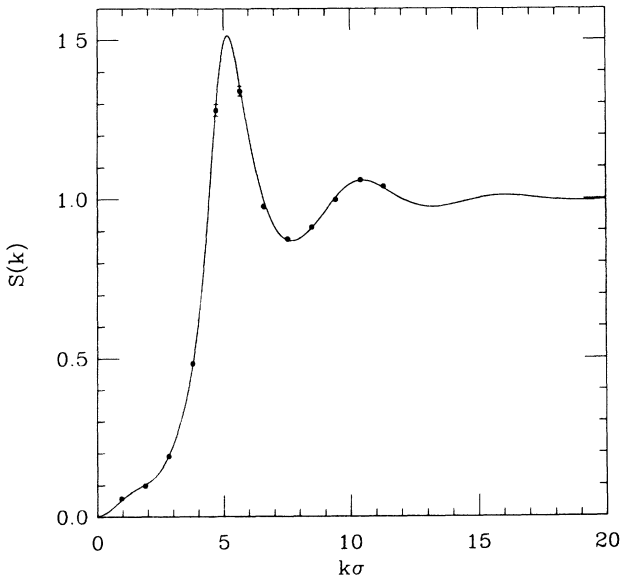

FIG. 4. The structure factor $S(k)$ of the shadow coordinates at the equilibrium density. The data with error bars are obtained from the shadow configurations; the Fourier transform of their pair correlation function is shown by the solid line.

At first glance, one possible solution should be to compute the same ratio of Eq. (22) but now displacing the shadow particles by the same amount that the real ones had being moved. It is a simple exercise to change variables in Eq. (1) and to see that this is a correct procedure. One can show, however, that this calculation has an infinite variance so that even a simple estimation of $n(r)$ is very difficult to make.

Because we have a more elaborate trial function than those previously studied, a more sophisticated technique, such as the one used by Ceperley and Pollack[26] in the context of path-integral calculations, is needed. The idea is to allow an extra atom off the diagonal, that is to perform a simulation where the integrand of Eq. (20) itself is sampled; the unnormalized probability distribution function (PDF)

$$\Psi_T(\mathbf{r}_1, \mathbf{r}_2, \ldots, \mathbf{r}_i', \ldots, \mathbf{r}_N)\Psi_T(\mathbf{r}_1, \mathbf{r}_2, \ldots, \mathbf{r}_i, \ldots, \mathbf{r}_N) , \tag{28}$$

is sampled by an independent random walk following the Metropolis prescription; $\mathbf{r}_i'$ and $\mathbf{r}_i$ are now independent, so the sampling has three extra dimensions. By using a binning procedure, one can then tabulate

$$n'(r)=\langle\delta(|\mathbf{r}_i'-\mathbf{r}_i-\mathbf{r}|)\rangle\ . \tag{29}$$

Finally, noting that $n(0)=1$, one may recover

$$n(r)=\mathcal{N}n'(r)\ , \tag{30}$$

The normalization factor $\mathcal{N}$ is obtained by extrapolation of the unnormalized $n'(r)$ to $r=0$.

In fact, to improve the statistical resolution of the algorithm, so that all the important points in the configuration space are taken into account regardless of the size of $r=|\mathbf{r}_i'-\mathbf{r}_i|$, we followed a further suggestion of Ceperley and Pollock and sampled instead

$$\frac{1}{r^2n_a(r)}\Psi_T(\mathbf{r}_1,\mathbf{r}_2,\ldots,\mathbf{r}_i',\ldots,\mathbf{r}_N)$$
$$\times\Psi_T(\mathbf{r}_1,\mathbf{r}_2,\ldots,\mathbf{r}_i,\ldots,\mathbf{r}_N)\ , \tag{31}$$

where $n_a(r)$ is an approximation to the single-particle density matrix that we take to be a Gaussian plus a constant. Of course in Eq. (29) the δ function must be multiplied by the same factor $r^2n_a(r)$ so that we still compute the same quantity. That is, the estimator for $n(r)$ is

$$n(r)=\mathcal{N}\langle r^2n_a(r)\delta(|\mathbf{r}_i'-\mathbf{r}_i-\mathbf{r}|)\rangle\ , \tag{32}$$

Without considering the normalization factor $\mathcal{N}$ our results for the single-particle density matrix are shown in Fig. 5. Although there is a long autocorrelation time in this calculation and we have to divide the whole curve by $n(0)$, the correct magnitude of the condensate fraction can be obtained directly from Fig. 5. A crude calculation could give a condensate fraction of approximately 4.6%.

To estimate the condensate fraction in a more precise way, the normalization factor $\mathcal{N}$ may be obtained in the following manner. As we mentioned before, Eq. (22) gives reliable results for $r<1\sigma$ and so the results obtained through it can be smoothly matched with the one displayed in Fig. 5. Taking into account this fact, we computed a normalization constant using the data of both curves, one calculated by Eq. (22) and the other obtained considering Eq. (32), in the range $0.3\sigma<r<0.7\sigma$. Our determination of the normalization constant gives $\mathcal{N}=5.551\pm0.016$. This result does not depend critically on the range. Finally, considering the data of Fig. 5 from $r=2.34\sigma$ to the side of the simulation box at $r=3.34\sigma$ we compute the condensate fraction as $n_0=0.0451\pm0.0003$.

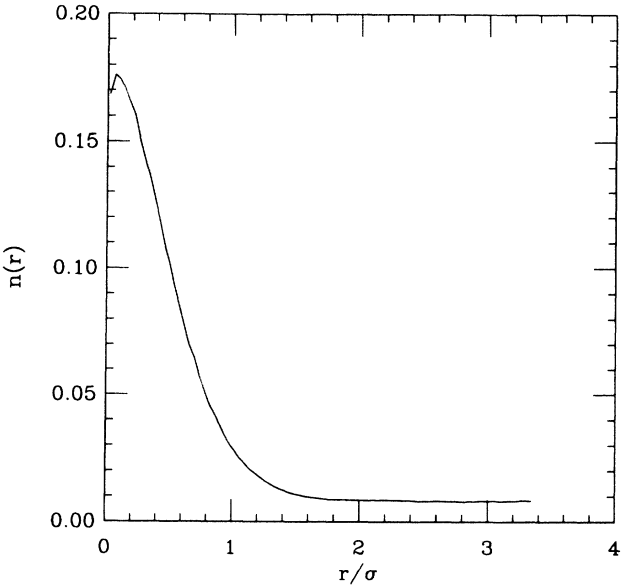

FIG. 5. The unnormalized single-particle density matrix computed at the equilibrium density with $n=9$ as the power law for the shadow model potential.

It is interesting to compare this variational result with the others obtained using different trial functions. For completeness, a comparison with GFMC is worthwhile. This is shown in Table III. Here again we have a further hint that our trial function implicitly includes enhanced three-body correlations. Although the condensate fraction measured with a wave function of the Jastrow form plus explicit three-body interactions gives results that are higher than the ones obtained with the shadow wave function, both results are substantially lower than the values determined from trial functions having a simple Jastrow form. From this we conclude that in achieving lower energies than the simple Jastrow form, both the shadow wave function and the wave function with explicit three-body correlations yield less accurate descriptions of the off-diagonal long-range order in the true ground-state wave function: both results are about a factor of 2 smaller than the established value from GFMC of $n_0=0.0935\pm0.0005$.[27] According to Whitlock[28] the results of Ref. 27 shown as the last row of Table III are in

TABLE III. Fraction of atoms condensed in the zero-momentum state at the equilibrium density, $\rho\sigma^3=0.365$. The trial functions indicated for GFMC results are the ones used as importance functions. The notation is the same as the one in Table II. The first line shows the result obtained with a shadow trial function (SH). All the calculations have been performed for systems of 108 particles.

	Variational	Green's-function Monte Carlo	
Ψ_T	n_0	n_0^{mixed}	$n_0^{\text{extrapolated}}$
SH	0.0451±0.0003		
J	0.0932±0.0003		
J(PPA)[a]	0.1069±0.0002	0.1002±0.0003	0.0935±0.0005
$J+T$[a]	0.0562±0.0005	0.0680±0.0004	0.0798±0.0008

[a]Reference 27.

fact less reliable because of a less than optimal choice of trial function. Much longer Monte Carlo runs than were made would have been required to achieve a reliable convergence for n_0.

V. THE SOLID PHASE

In this work, we used the shadow wave function to study for the first time the recrystallization of a configuration of ^{4}He atoms half of which had been melted to a liquidlike state (see Sec. VI). From this we infer that one could start from any reasonable configuration, say a liquid, and if the right values of the variational parameters were used, then by waiting long enough, one would eventually reach an equilibrated crystalline state. Of course if we start from a perfect crystalline structure the equilibrium state of the system as a solid will be obtained much more rapidly. As a matter of convenience we have begun the simulations reported in this section from the same fcc lattice that was used at the beginning of the simulations in the liquid phase. Using this procedure, the equilibrium state was quickly obtained.

For the crystal phase of ^{4}He the variational energy was computed using 108 particles at the densities $\rho\sigma^3=0.55$ and 0.491. The latter is the melting density determined[16] by GFMC. At $\rho\sigma^3=0.55$ three different power laws have been tested for the model potential $v(s)$, Eq. (7). The results are shown in Table IV, and they are less sensitive to the exact form of the model potential of the shadow coordinates than those obtained for the fluid phase.

Using the Aziz potential and a standard Nosanow-Jastrow (NJ) wave function—a Jastrow factor multiplied by a product of Gaussian localization factors that bind the atoms to fcc lattice sites—we have computed the variational energy and it is presented in Table V. The optimization of this wave function requires the variation of the parameters b and C, cf. Eqs. (4) and (5). In this last equation, for the NJ trial function, the value $\mathbf{s}_k$ are just the fcc lattice sites. Our best variational energy for this trial function is obtained for $b=1.10\sigma$ and $C=4.8\sigma^{-2}$. It is also useful to quote results determined with a more elaborate trial function and by the GFMC method.

If we compare the energies obtained with the shadow wave function with that found from Nosanow-Jastrow, we see that the first trial function gives significantly lower values. Now let us consider the difference between GFMC and variational results determined in the liquid and in the solid phase. If we do this first with a trial function of the Jastrow form plus explicit three-body correlations we see that this difference is constant at about 0.4 K. Making the same calculation for the shadow wave function we see that although in the liquid phase this difference is 0.9 K it is lowered to 0.7 K in the solid phase. This fact suggests that this description of the actual system by the shadow wave function is improved when we go from the liquid to the solid phase.

TABLE V. Results for the crystalline phase obtained at $\rho\sigma^3=0.55$ for ^{4}He. In the first column we give the trial or importance junction used. The Nosanow-Jastrow wave function is indicated by NJ, and a Nosanow-Jastrow function plus explicit triplet correlations by NJ+T. In the following columns we show, respectively, the variational energies, the variational Lindemann ratio, and finally the mixed-energy estimator for the GFMC calculation. The GFMC result has been interpolated using the equation of state of Ref. 16; although we do not give an error, it should not exceed 2%. All the calculations have been performed for systems for 108 particles. The energies are presented in K per atom.

Ψ_T	$E_T^{\rm var}$	Lindemann ratio (variational)	$E^{\rm mixed}$ [a]
NJ	-3.322 ± 0.019	0.22	-4.23
NJ+T [b]	-3.786 ± 0.014		

[a]Reference 16.
[b]Reference 28.

In the crystal phase we have computed Lindemann's ratio. This quantity is defined as the quotient of the square root of the second moment of the single-particle distribution function divided by the nearest-neighbor distance. Results are shown in Tables IV and V, with Table V containing the values obtained from a NJ wave function. The Lindemann ratios of the shadow particles are given in Table IV. Here the l_i in Eq. (23) are the lattice positions shifted by the distance by which the center of mass of the shadows has diffused. The values for the Lindemann ratio of the actual quantum system, described by the real particles, has a value around 0.23, that is characteristic of quantum solids at these densities.[13] As one expects, the shadow coordinates have a much smaller value, one typical of a classical solid. For example, the classical Lennard-Jones system near melting has Lindemann ratio near 0.14.[29]

The wave function discussed here has been shown analytically[3] to have a Bose-Einstein condensation in the solid phase. The condensate is positive although it could be very small. Our calculations did not show evidence of such a condensate. One possible reason for this result is

TABLE IV. Variational energies and Lindemann ratios obtained with the shadow wave function for the crystalline phases at two densities. The same units of Table I are used.

		Lindemann ratio		Parameters			
$\rho\sigma^3$	E_T	Real	Shadow	b	$b_{\rm sh}$	n	C
0.491	-5.004 ± 0.055	0.25	0.18	1.10	1.70	5	4.8
0.55	-3.521 ± 0.032	0.23	0.16	1.10	1.67	5	5.7
0.55	-3.529 ± 0.027	0.23	0.13	1.10	1.35	9	5.7
0.55	-3.563 ± 0.031	0.22	0.13	1.09	1.28	12	5.7

that it takes a very long simulation to allow exchange between the shadows and thus to get a positive condensate. Perhaps if one rewrites the wave function in a way in which each of the real particles is explicitly coupled to *all* the shadows it would be possible to measure the condensate fraction in a shorter amount of computer time.[30] We have not yet explored this possibility.

Our failure to see a condensate does not imply that in calculating properties of the crystal we are in fact violating the symmetry of the original trial function as it is considered in Sec. II. If we take into account the crystallization experiments of the next section we can make the following remarks. During the evolution from a liquidlike configuration to one of a solid, all configurations could be sampled. In this process the system will choose the most important configurations, and finally reach, as we want, equilibrium as a solid. Specifically we want the shadow particles, the part of the wave function that provides the interaction for solidification, to reach and then remain in a crystal structure. Besides there is no constraint that prevents exchange between the shadow particles, even though the exchanges are likely to be infrequent. In another words, during the simulations the system can be in any of its configurations, and so we can say that the symmetry of the wave function, as well as its independence of an *a priori* lattice, has been probed.

The single-particle density $\rho(\mathbf{r})$ about a lattice site is of interest since in our wave function we do not have any explicitly prescribed lattice sites. The spherical average of this single-particle density $\rho(r)$ has been computed for the real particles and the shadow coordinates using Eq. (23). Figure 6 presents both $\rho(r)$ on a semilog plot at the density $\rho\sigma^3=0.55$. The behavior of both curves are nearly Gaussian. This conclusion can also be drawn from Table VI, where we give the first three moments of $\rho(r)$, the ratios $\langle r^4\rangle/\frac{5}{3}\langle r^2\rangle^2$ and $\langle r^6\rangle/\frac{105}{27}\langle r^2\rangle^3$ for two different densities. These ratios are unity for a perfect Gaussian distribution. Results for the angular dependence of $\rho(\mathbf{r})$ are desirable since in classical hard-sphere systems considerable anisotropy is present[31] and we expect the shadows to behave like classical particles. We are presently performing such simulations in an effort to compare with recent experiments attempting to measure the anisotropy in solid helium.[32]

The results at $\rho\sigma^3=0.55$ from the NJ wave function, the shadow wave function, and path-integral Monte Carlo are compared in Table VII. We performed the path-integral Monte-Carlo (PIMC) simulation at a temperature of 4 K along the lines of Pollock and Ceperley's work.[33] The PIMC method gives essentially exact results within statistical error and so may be used to test the relative merits of the various trial wave functions. PIMC is inapplicable at zero temperature, but does not involve the use of a trial or importance function. It is thus complementary to variational and to GFMC when it can be used at a low enough temperature so that results may be extrapolated reliably to zero. From Table VII one sees that the optimal shadow wave function does better than the optimal NJ wave function in predicting the three moments $\langle r^2\rangle$, $\langle r^4\rangle$, and $\langle r^6\rangle$. The NJ wave function underestimates $\langle r^2\rangle$ by about 20% whereas the shadow wave function is only off by 10%. We estimate[12] that the effect of finite temperature in the PIMC calculation raises $\langle r^2\rangle$ by about 5% above the actual $T=0$ value. Thus the correlation for this fact brings the shadow wave function results into even closer agreement with the exact values. A similar improvement should occur in the higher moments as well. The three calculations shown in Table VII predict small but statistically significant deviations from Gaussian behavior in the moments $\langle r^4\rangle$ and $\langle r^6\rangle$. This is indicated by the difference from unity of the ratios in the last two columns. The NJ and shadow wave functions give nearly the same values for the ratios, both underestimating the PIMC results. From the results discussed in this paragraph, we conclude that the shadow wave function more accurately describes the single-particle distribution about a lattice site than does the standard NJ wave function.

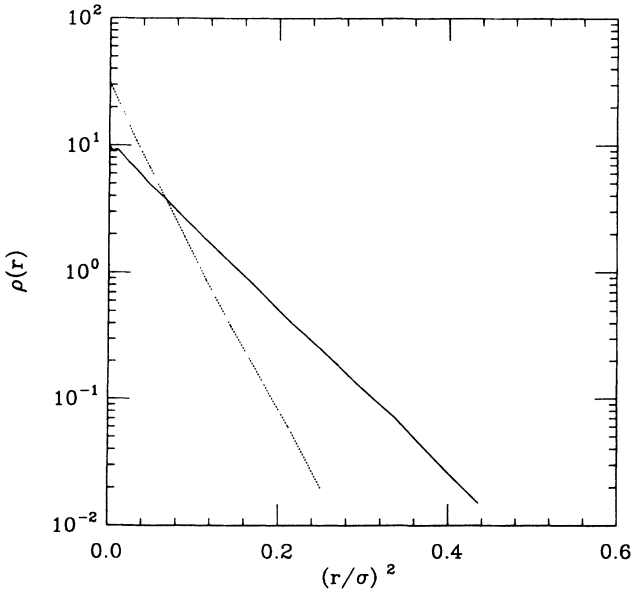

FIG. 6. Spherical average of the single-particle density function for displacements from a lattice site at density $\rho\sigma^3=0.55$ for the real particles, solid line. For the shadow coordinates this quantity is shown by the dashed line.

TABLE VI. Moments of the single-particle distribution $\rho(r)$ and the indicated ratios of these moments at the given densities $\rho\sigma^3$ obtained with the shadow wave function. The lengths are in units of σ. The ratios are unity for a Gaussian distribution.

$\rho\sigma^3$	$\langle r^2\rangle$	$\langle r^4\rangle$	$\langle r^6\rangle$	$\frac{\langle r^4\rangle}{\frac{5}{3}\langle r^2\rangle^2}$	$\frac{\langle r^6\rangle}{\frac{105}{27}\langle r^2\rangle^3}$
0.491	0.126±0.009	0.0267±0.002	0.0081±0.0006	1.017±0.0016	1.053±0.006
0.55	0.0997±0.007	0.0168±0.001	0.0040±0.0003	1.014±0.0017	1.042±0.005

TABLE VII. Values obtained using the Nosanow-Jastrow (NJ) wave function, the shadow wave function (SH), and the path-integral Monte Carlo method (PIMC) for the moments of the single-particle distribution $\rho(r)$ and the two indicated ratios of these moments at $\rho\sigma^3=0.55$. The lengths are in units of σ. The ratios are unity for a Gaussian distribution.

	$\langle r^2\rangle$	$\langle r^4\rangle$	$\langle r^6\rangle$	$\frac{\langle r^4\rangle}{\frac{5}{3}\langle r^2\rangle^2}$	$\frac{\langle r^6\rangle}{\frac{105}{27}\langle r^2\rangle^3}$
NJ	0.0903±0.006	0.0138±0.0010	0.0030±0.0002	1.016±0.0016	1.051±0.006
SH	0.0997±0.007	0.0168±0.0010	0.0040±0.0003	1.014±0.0017	1.042±0.005
PIMC	0.109±0.001	0.0204±0.0005	0.0055±0.0001	1.025±0.0005	1.080±0.001

VI. CRYSTALLIZATION

Using the shadow wave function, we have conducted several simulations starting from an equilibrated liquid configuration of the system in order to see whether the system would eventually crystallize. In these runs we have considered systems with 108, 324, and 864 particles. The final results were drawn mostly from experiments on the larger system in order to diminish the role played by periodic boundary conditions. We watched the evolution of the system by tabulating at every Metropolis "pass' the structure function $S(k)$, computed from Eq. (19), near the its first maximum.

The simulations were started from a fcc lattice. Then, a fraction of the system was "melted." That is, a subset of the particles were allowed to equilibrate as a liquid using an appropriate set of parameters in the shadow trial function. The remainder of the system was kept fixed, so it retained its perfect lattice structure. This part constituted the seed for the crystallization process. The structure function normalization is such that at the first maximum for the perfect lattice, $S(k)$ is equal to the number of fixed particles. Prior to the equilibration towards the liquid phase, the corresponding value of $S(k)$ for the fraction of the system that melted was also equal to the number of particles involved. The value of $S(k)$ was computed for $\mathbf{k}$ in the plane parallel to the surface that separates the two phases.

Now we will describe in detail one simulation performed with 864 particles at $\rho\sigma^3=0.55$. Half of the system was equilibrated as a liquid using 500 passes. In Fig. 7 we present the evolution of this half as indicated by $S(k)$ near its fixed maximum; the first few passes are not shown in the figure. In the other part, the particles were kept fixed so that if this same calculation were made, we would obtain the constant value of $S(k\sigma=5.66)=432$. After these 500 passes, the whole system was allowed to evolve with the parameters of Table IV for $n=5$. The same analysis was started again for the particles in the liquidlike configuration in equilibrium. The result is displayed in Fig. 8. From this figure, it is evident that the system recovered its structure, reaching a saturation point after 4500 passes.

To learn if the system actually crystallized, we made a control run of 1000 passes where the whole system was allowed to equilibrate starting from an fcc lattice. This control run was performed at the same density $\rho\sigma^3=0.55$ and using the same set of parameters for the solid phase. We recorded the structure function $S(k)$ near its first maximum for half of the simulation box. The results of the analysis of the control run are shown in Fig. 9 together with the last 1000 passes displayed in Fig. 8. In the control run, first we have an equilibration of the perfect lattice, so that the initial value of $S(k\sigma=5.66)=432$ drops. If we examine Fig. 9, we can see that the mean equilibrated value of $S(k\sigma=5.66)$ in the control run is the same as the average value in the run that starts from the liquidlike configuration. To gain a quantitative confirmation of this result we adopted the following procedure. In the control run we blocked the value of $S(k\sigma=5.66)$ in the last 500 passes into five blocks and computed the average value and its error. We obtained the result 102±2. The same procedure was done in the run where we achieved crystallization. The mean value of $S(k\sigma=5.66)$ in this case was 101±2, in agreement with the control run.

In the systems with 108 and 864 particles the size of the crystallization seed was varied in our experiments. When we began with $\frac{2}{3}$ of the system equilibrated as a liquid, we were not able to see crystallization during the runs we made. Monitoring the particles that form the

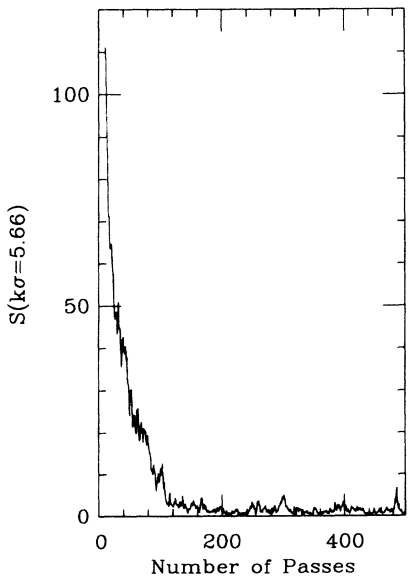

FIG. 7. The evolution of the structure function for 432 particles during the period of equilibration towards a liquidlike configuration. The first few passes are not shown.

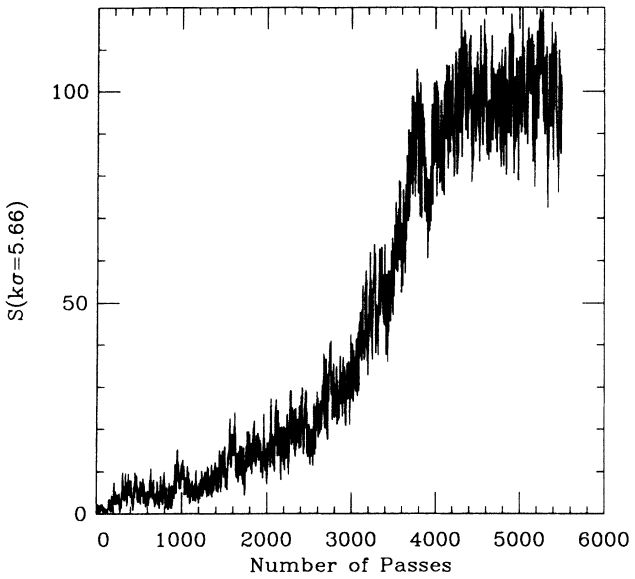

FIG. 8. Evolution of the liquidlike configuration to a crystalline phase. The variational parameters are those appropriate for the crystalline phase at $\rho\sigma^3=0.55$ and $n=5$.

crystallization seed shows that they lost their lattice structure so that the system could not crystallize. On the other hand, when $\frac{1}{3}$ was equilibrated as a liquid, the system as a whole arrived at a crystalline state after a suitable number of passes and when the appropriate variational parameters were used. We do not believe that the lack of crystallization for the smaller seed is significantly different from what would be obtained in similar Monte Carlo experiments of classical systems with fixed volume, since even for these systems a crystal is not always obtained. In our experiments the order in which the particles were moved in each pass was randomized to assure that the crystallization was not an artifact of some particular order of attempted moves.

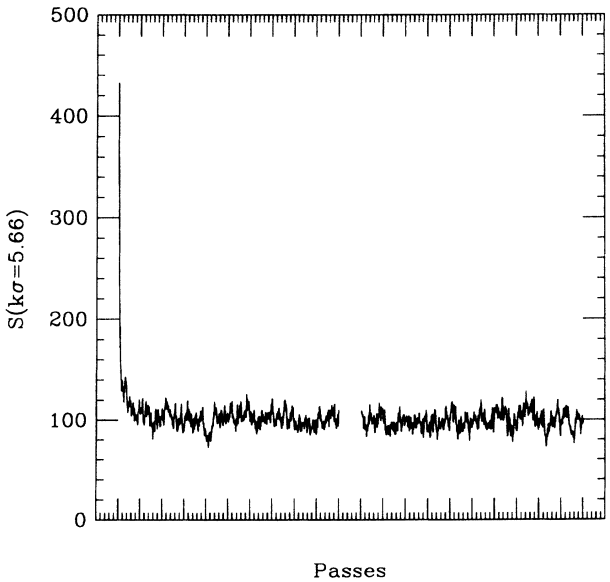

FIG. 9. Comparison between the evolution of the system starting from a perfect fcc lattice (left) and the last 1000 passes of the recrystallization process (right). The distance between major tick marks along the x axis denotes 100 passes.

In the thermodynamic limit one expects that crystallization will occur for seeds with a critical size that is only a small fraction of the whole system. We were successful in obtaining crystallization with a system in which fewer than half of the particles constituted the seed. This was done for a system with 324 particles in which 144 were kept as the initial seed. In this experiment we used a simulation box with nine unit cells on one side and three on the other two. Our results show that after 6800 passes the whole system became a solid. No attempt to determine the critical size of the crystalline seed has been made.

Our results[34] for the crystallization of a two-dimensional system are very different from those that we report here for the three-dimensional case in regard to the crystallization seed. In two dimensions we do not need such a seed to achieve crystallization. This result is not entirely unexpected because of the very similar results that have been seen in two-dimensional classical simulations.[35]

VII. DISCUSSION

In this work we have shown that the "shadow" wave function is a reliable trial function to compute variational ground-state energies. It can also be used to describe an effect that was out of the question in previous variational studies, viz., crystallization during a Monte Carlo simulation. Although our wave function still requires a seed for the crystallization process, it is able to give the correct structure in the solid phase when we begin with an equilibrated liquidlike configuration. Other properties of interest in the liquid and solid phases of ^{4}He can be evaluated as well. In addition, the wave function overcomes some of the deficiencies present in previous variational calculations. With this trial function we are able to restore Bose symmetry, along with translation invariance, and we do not need the *a priori* introduction of a lattice in the solid phase. In the liquid phase, correlations in the wave function among the particles are enhanced to all orders as compared to the pure pairwise Jastrow form. The important three-body correlations[5,36,37] in helium systems are at least partially present in the shadow wave function. The only difficulty that remains is that the system appears unable, for runs of the length that we have considered, to evolve from one lattice structure to another. This is in part due to the fact that relatively small systems obeying periodic boundary conditions were used.

Another point worth noting is that a fixed functional form of the wave function is used in both liquid and solid phases. The properties of the system are determined by the choice of parameters in the wave function rather than by varying its functional form as was done in previous work. We note that from Tables I and IV there is a fairly smooth change of the variational parameters with density, even through the phase transition. For example, the coexisting liquid and solid densities ($\rho\sigma^3=0.438$ and

0.491, respectively) differ by about 10% and our variational parameters change by roughly the same amount. Further experimentation is necessary to determine whether the optimal shadow wave function is actually continuous through the coexistence region.

We believe that wave functions of the shadow type can be used to explore some additional important low-temperature phenomena. In collaboration with Luciano Reatto we plan to use them to study defects in quantum crystals as well as to compute the excitation spectrum of the liquid phase. It appears to be possible to construct an analog of Penrose's finite-temperature density matrix based upon shadow wave functions. One can also devise a shadow wave function with a net angular momentum that describes a quantum vortex while permitting a nonzero density of atoms on the vortex core.

Finally, we note that we are dealing with a new ansatz to treat many-boson systems. We expect that new insights on the nature of these and related quantum systems will be realized through the shadow wave function.

ACKNOWLEDGMENTS

We would like to acknowledge many useful discussions with D. M. Ceperley, L. Reatto, K. E. Schmidt, and P. A. Whitlock. We thank P. A. Whitlock for permission to quote some results prior to publication. This work was partially supported by the Condensed Matter Theory Program of the National Science Foundation under Grant No. DMR-8419083, by the Advanced Scientific Computing Program of the National Science Foundation (NSF) under Grant No. ASC-8715641. It was conducted using the Cornell National Supercomputer Facility, a resource of the Center for Theory and Simulation in Science and Engineering at Cornell University, which is funded in part by the National Science Foundation, New York State, and the IBM Corporation.

[1]Silvio Vitiello, Karl Runge, and Malvin H. Kalos, Phys. Rev. Lett. **60**, 1970 (1988).
[2]R. Jastrow, Phys. Rev. **98**, 1479 (1955).
[3]L. Reatto and G. L. Masserini, Phys. Rev. B **38**, 4516 (1988).
[4]W. L. McMillan, Phys. Rev. **138**, A442 (1965).
[5]K. Schmidt, M. H. Kalos, M. A. Lee, and G. V. Chester, Phys. Rev. Lett. **45**, 573 (1980).
[6]J. P. Hansen and D. Levesque, Phys. Rev. **165**, 293 (1968).
[7]L. H. Nosanow, Phys. Rev. Lett. **13**, 270 (1964).
[8]R. P. Feynman and A. R. Hibbs, *Quantum Mechanics and Path Integrals* (McGraw-Hill, New York, 1965).
[9]D. Chandler and P. G. Wolynes, J. Chem. Phys. **74**, 7 (1981).
[10]K. S. Schweitzer, R. M. Stratt, D. Chandler, and P. G. Wolynes, J. Chem. Phys. **75**, 3 (1981).
[11]Y. J. Wong and G. V. Chester, Phys. Rev. B **37**, 9590 (1988).
[12]K. J. Rugge and G. V. Chester, Phys. Rev. B **38**, 135 (1988).
[13]P. A. Whitlock, D. M. Ceperley, G. V. Chester, and M. H. Kalos, Phys. Rev. B **19**, 5598 (1979).
[14]M. H. Kalos and P. A. Whitlock, *Monte Carlo Methods* (Wiley, New York, 1986).
[15]R. A. Aziz, V. P. S. Nain, J. S. Carley, W. L. Taylor, and G. T. McConville, J. Chem. Phys. **70**, 4330 (1979).
[16]M. H. Kalos, M. A. Lee, P. A. Whitlock, and G. V. Chester, Phys. Rev. B **24**, 115 (1981).
[17]N. Metropolis, A. W. Rosenbluth, M. N. Rosenbluth, A. H. Teller, and E. Teller, J. Chem. Phys. **21**, 1087 (1953).
[18]Silvio Vitiello, Karl Runge, and Malvin H. Kalos, in *Nuclear and Atomic Physics at One Gigaflop*, edited by J. B. McGrory, M. R. Strayer, and C. Bottcher (Harwood Academic, Chur, Switzerland, 1988).
[19]O. Penrose and L. Onsager, Phys. Rev. **104**, 576 (1956).
[20]F. J. Pinski and C. E. Campbell, Phys. Lett. **78B**, 23 (1978).
[21]D. M. Ceperley and M. H. Kalas, in *Applications of the Monte Carlo Methods in Statistical Physics*, edited by K. Binder (Springer-Verlag, Berlin, 1984).
[22]D. M. Ceperley and G. V. Chester, Phys. Rev. A **15**, 755 (1977).
[23]E. C. Svensson, V. F. Sears, A. D. B. Woods, and P. Martel, Phys. Rev. B **21**, 3638 (1980).
[24]F. H. Wirth and R. B. Hallock, Phys. Rev. B **35**, 89 (1987).
[25]J. P. Hansen and L. Verlet, Phys. Rev. **184**, 151 (1969).
[26]D. M. Ceperley and E. L. Pollack, Can. J. Phys. **65**, 1416 (1987).
[27]R. M. Panoff and P. A. Whitlock, in *Momentum Distributions*, edited by R. N. Silver and P. E. Sokol (Plenum, New York, 1989).
[28]P. A. Whitlock (private communication).
[29]J. P. Hansen and I. R. McDonald, *Theory of Simple Liquids* (Academic, London, 1976).
[30]L. Reatto (private communication).
[31]P. A. Young and B. J. Alder, J. Chem. Phys. **60**, 1256 (1974).
[32]R. O. Simmons (private communication).
[33]E. L. Pollock and D. M. Ceperley, Phys. Rev. B **30**, 2555 (1984).
[34]Silvio Vitiello, Karl Runge, and Malvin H. Kalos, in *Computer Simulation Studies in Condensed Matter Physics: Recent Developments*, edited by D. P. Landau and H. B. Schuttler (Springer-Verlag, Berlin, 1988).
[35]Y. J. Wong and G. V. Chester, Phys. Rev. B **35**, 3506 (1987).
[36]V. R. Pandharipande, Phys. Rev. B **18**, 218 (1978).
[37]C. C. Chang and C. E. Campbell, Phys. Rev. B **15**, 4238 (1977).